Hindawi
Advances in Materials Science and Engineering
Volume 2018, Article ID 9690202, 11 pages
https://doi.org/10.1155/2018/9690202

Research Article

Nonlinear Bond Model for the Dowel Action considering the Fatigue Damage Effect

Pengfei Li, Ni Tan, and Chengzhi Wang

Department of Harbor, Waterway and Coastal Engineering, Chongqing Jiaotong University, Chongqing 400074, China

Correspondence should be addressed to Chengzhi Wang; wangcz@cqjtu.edu.cn

Received 6 April 2018; Accepted 28 May 2018; Published 20 June 2018

Academic Editor: Aniello Riccio

To investigate the mechanical properties of dowel action under fatigue loads, 3 reinforced concrete specimens with different bar diameters (12 mm, 20 mm, and 25 mm) were subjected to the fatigue loading and were designed to investigate the attenuation character of dowel action and the fatigue failure modes. The load transfer mechanism of the bond was analyzed based on the 3D relative motions between reinforcing bars and subgrade concrete. Fatigue damage effects were considered in the model. A deterioration coefficient based on the deformation path was defined to represent the accumulation of fatigue damage. Verification of the model was conducted by comparing the analysis results with experimental data obtained in this study and from the literature, and satisfactory agreement was obtained.

1. Introduction

The dowel action is one of the main mechanisms of load transfer along the interfaces. These interfaces and joints may turn out to be critical planes in the operation of the load-resisting mechanism and thus may govern the ultimate strength, ductility, and energy absorption capacity of an entire structure [1–4]. As the important components of reinforced concrete structures, structural joints are directly subjected to shear loads of great magnitude and cycles. During their service life, the mechanical performances of dowel action gradually degrade due to the high cycle repetition of loads which might cause the sudden collapse of the entire structure. Therefore, the mechanical behavior of dowel action under fatigue loads should be taken into account.

In recent years, extensive experimental and analytical investigations have been carried out to study the mechanical properties of the dowel action [5–7]. Vintzeleou and Tassios [8] experimentally investigated the behavior of dowels under cyclic deformation. Test results indicated that both the bearing capacity and the stiffness of dowel action show obvious degradation, especially in case of full reversed deformations. Mattock and Hawkins [9] carried out a series of high cycle fatigue tests of push-off specimens. The relation between dowel shear force and transverse shear slip for various cycle totals of specimen under different loading levels were obtained.

A number of finite element (FE) models have been developed for the analysis of the dowel action [10–14]. Soltani and Maekawa [1] developed a path-dependent RC interface model under a multidirectional displacement path. Moradi et al. [15] presented a simplified model for the dowel action by suggesting a simple formula for subgrade springs. Maekawa and Qureshi [16, 17] proposed an enhanced computational model for the prediction of reinforcing bar behaviors under generic conditions of axial and transverse displacements. A unified model for RC interface stress transfer was presented based on a combination of a generic bar model and a physical model for aggregate interlock [18]. An open-slip coupled model was developed to simulate the bond behavior of reinforcing bars in concrete [19] and was later extended to cover the cored reinforcement [20]. The author developed a bond model considering the coupled damage effect. Both the effect of the crushing of the concrete supporting the bar and the strain effect are considered in the analysis [21]. However, the mechanical behavior of dowel action under fatigue loads has yet to be considered.

Table 1: Mixture proportion of concrete.

Water (kg/m^3)	Cement (kg/m^3)	Coarse aggregate (kg/m^3)	Fine aggregate (kg/m^3)	Plasticizer (kg/m^3)	Water-cement ratio
195	415	1146	644	0.57	0.47

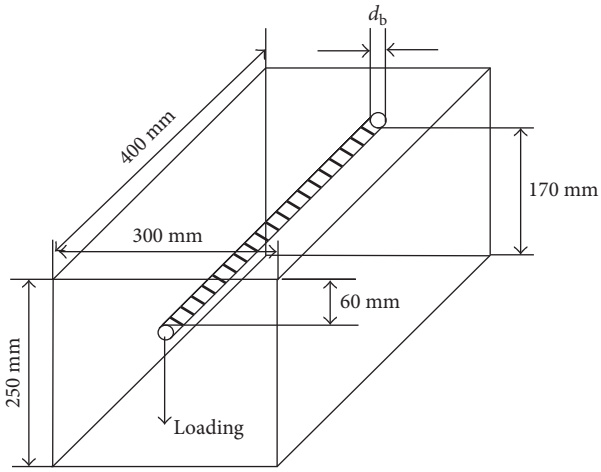

Figure 1: Dimensions of specimen.

Recently, research progress has been made on the fatigue life assessment of reinforced concrete structures with finite element methods (FEMs) [22]. Nonlinear fatigue constitutive models of concrete intension, compression, and shear along crack planes were formulated and have been verified experimentally. To accelerate the computation for huge numbers of fatigue cycles, a direct path-integral scheme is also proposed for the fatigue simulation of long time range. This framework has been further enhanced for the simulation of bridge slab performance under high cycle moving loads [23, 24]. Therefore, these life assessment schemes could be used to solidify the quantitative background of the bond model considering the fatigue damage effect.

The objective of the present study is to develop a 3D bond model to predict the behavior of dowel action under fatigue loads. The effect of fatigue damage on the behavior of the dowel action is introduced, and a deterioration coefficient is chosen to characterize the damage level. Three block-type specimens were subjected to fatigue loads and were designed to investigate the attenuation character of dowel action and the fatigue failure modes. To demonstrate the versatility of the proposed model, verification is conducted by comparing analysis results with experiments.

2. Experimental Program

2.1. Materials and Mixtures. The concrete mixture shown in Table 1 was adopted in the present study. The components consisted of ordinary Portland cement (PO 42.5), coarse aggregate with a maximum gravel diameter of 20 mm, fine aggregate with a fineness modulus of 2.6, and polycarboxylate-based superplasticizer. The design yield strength of the bar is 400 MPa.

Table 2: Details of specimens subjected to fatigue loads.

Specimen	d_b (mm)	f'_{cc} (MPa)	V_{f1} (kN)	V_{f2} (kN)
D12-F	12	49.6	1.0	7.0
D20-F	20	50.1	1.0	18.0
D25-F	25	50.8	1.0	28.0

2.2. Specimen Design. In this study, a direct shear test approach is chosen to control the load path and obtain the transverse displacement. Three block-type specimens with the dimension of 400 mm (length) × 300 mm (width) × 250 mm (height) were cast, with each specimen being reinforced with a deformed bar, as shown in Figure 1.

As summarized in Table 2, 3 bar diameters (12 mm, 20 mm, and 25 mm) were adopted in this study. The specimens were subjected to the fatigue loading to investigate the mechanism of fatigue deterioration and the fatigue failure modes. For the fatigue test, a repeated single-sided shear force was applied to the dowel bar. The maximum load level (V_{f2}) was set equal to the 55% of the static capacity obtained from the monotonic tests [21], and the minimum load level was set as 1 kN (V_{f1}) in order to keep the specimen stable.

2.3. Test Setup and Measurement Scheme. The test setup is presented schematically in Figure 2. Two servohydraulic actuators with loading capacities of 250 and 150 kN were used in the loading frame, which allows both shear and axial forces to be applied to the dowel bar. The loading path is shown in Figure 3. Firstly, three static loading cycles were performed to eliminate the influence of the deformation of support device. Then, a number of fatigue cycles ($N = 100$, 1000, 10000, 20000, 40000, 60000, 80000, and 100000) were carried out. A force-controlling mode was adopted for fatigue loading, and the loading frequency was set as 2 Hz. After 100000 fatigue cycles, the specimen was tested up to failure to measure the residual carrying capacity.

In all tests, the shear displacements and shear forces were continuously recorded during loading with a data acquisition frequency of 1 Hz. Furthermore, several LVDTs were used to monitor the concrete block at different positions and to measure possible rigid body displacements of the specimen with respect to the loading frame.

2.4. Experimental Results. Figure 4 shows the dowel force-dowel displacement curves of specimen D12-F. The residual carrying capacity after 100000 fatigue cycles is 9.2 kN, less than the static capacity (11.6 kN for monotonic test [21]). It could be concluded that the accumulated fatigue damage due to fatigue loads will reduce the ultimate bearing capacity

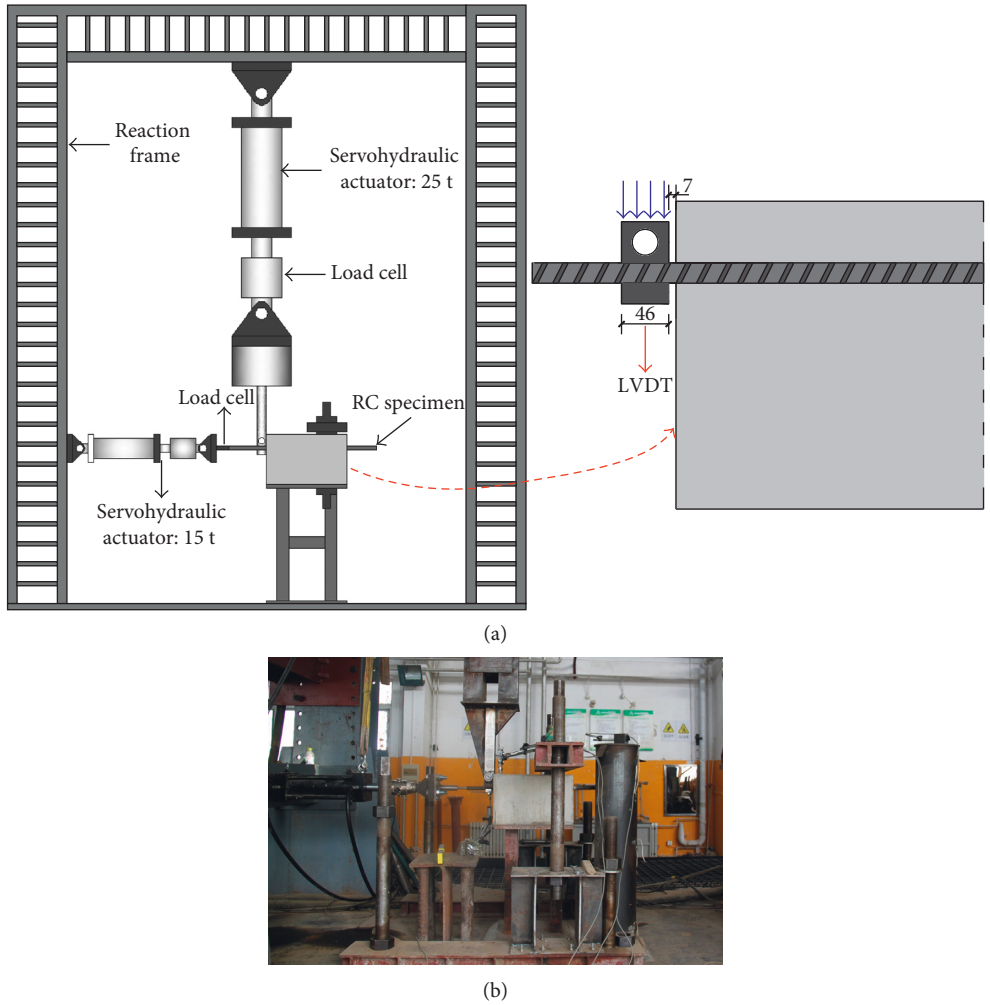

Figure 2: Schematic of test setup: (a) loading scheme; (b) measurement scheme.

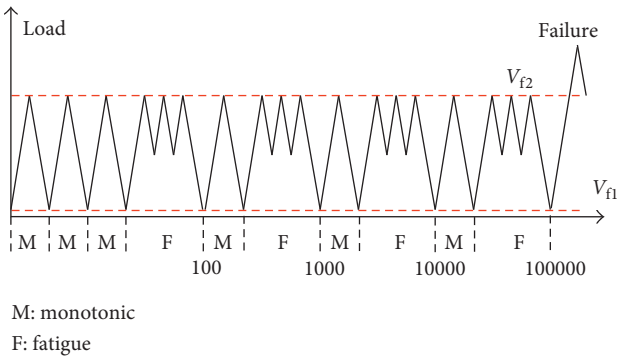

Figure 3: Loading path of fatigue tests.

of dowel action. This experimental phenomenon is of great significance to practical engineering design.

Load-displacement curves for specimens D20-F and D25-F are shown in Figures 5 and 6, respectively. The displacement of dowel bar at both the maximum load level and the minimum load level increase as the number of cycles increases. Reinforcing bar of specimens D20-F and D25-F

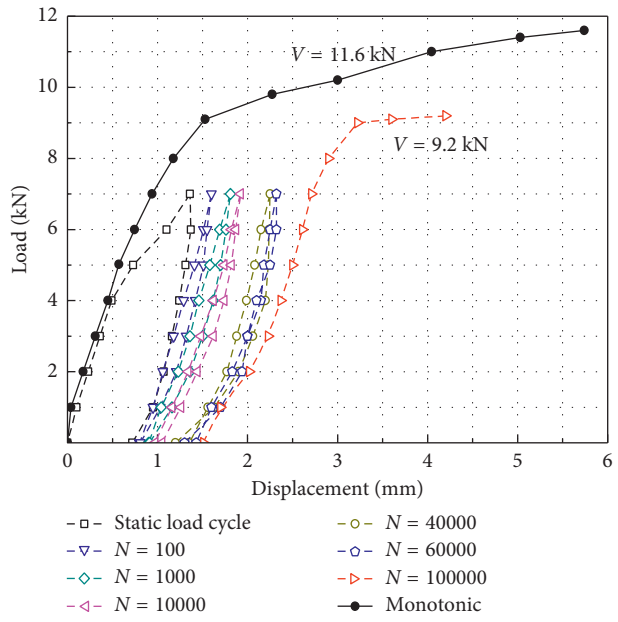

Figure 4: Load-displacement curves for specimen D12-F.

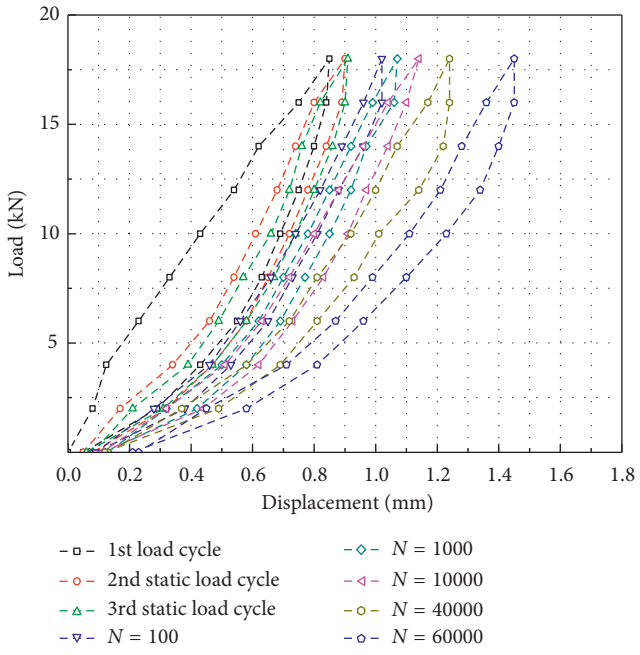

Figure 5: Load-displacement curves for specimen D20-F.

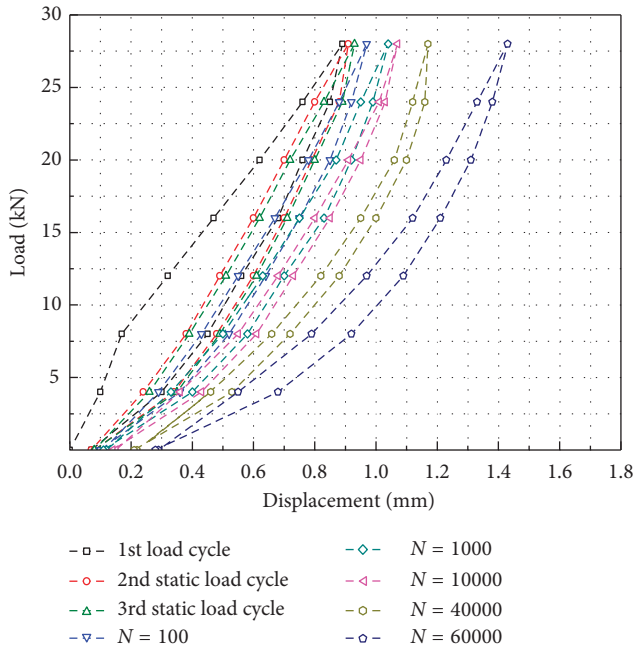

Figure 6: Load-displacement curves for specimen D25-F.

were ruptured at the 68720 and 72485 fatigue cycles. The position of facture was located about 1 times the bar diameter away from the surface of the specimen. Figure 7 shows the typical failure mode of these specimens. It could be concluded that the fatigue failure mode of dowel action is the fatigue rupture of the dowel bar, and the fatigue life is determined by the fatigue properties of steel and concrete.

Figure 8 shows the incremental displacement against the number of fatigue cycles. There exists a linear relation between incremental shear displacement and the logarithm of the number of fatigue cycles. This is similar to the S-N diagram for the fatigue life of materials which is in agreement with previous published results [9]. For specimens D20-F and D25-F, when the number of cycles is less than 40000, similar trends were presented to specimen D12-F, a linear relation between incremental shear displacement and the logarithm of the number of fatigue cycles was obtained. When the number of fatigue cycles is equal to 60000, there was a sudden increase in the shear displacement of the dowel bar and the stiffness degradation is obviously observed.

Based on the test data, the fatigue failure process of dowel action could be divided into two stages: the accumulation of fatigue damage and the fatigue rupture of dowel bar. In the former stage, the fatigue damage of materials gradually accumulated under fatigue loads. In the latter stage, the bearing section of dowel bar was fractured due to the growth and propagation of the microcracks in steel.

3. Constitutive Model of the Bond Behavior

3.1. Mechanical Mechanism of Three-Dimensional Relative Motions. To simulate the mechanical property of the dowel action, a three-dimensional bond model considering the coupled damage has been developed [21]. In which, the three-dimensional relative and the damage effect caused by both the micro radial cracks and the localized crushing of the surrounding concrete were integrated. A discrete FE method is adopted in this research. Both the steel bar and concrete are modelled by three-dimensional solid elements, and interface elements with zero thickness are used to describe the effect of the bond transition zone [20, 21]. Fatigue loads carried by reinforcing bars are transferred through this transition zone to the surrounding concrete.

In this paper, the basic methodology of previous work [21] was used and the damage equation of fatigue loads was analyzed. As shown in Figure 9, the three-dimensional relative motions can be resolved into 3 directions, namely, the normal direction, hoop direction, and axial direction. In the normal direction, the opening and closing of the interface represent the compression and separation between the dowel bar and the surrounding concrete due to the bending deformation of the dowel bar under shear loading. The bond stress field can be computationally summarized as follows [21]:

$$\tau_a = \frac{1}{L}\left(\sigma_a \sin\theta + \tau_a' \cos\theta\right),$$

$$\tau_n = G_n \delta, \tag{1}$$

$$\sigma_n = \frac{1}{L}\left(-\sigma_a \cos\theta + \tau_a' \sin\theta + \sigma_n'\right),$$

where τ_a is the bond stress in the axial direction, σ_n is the total normal stress, τ_n is the hoop stress, δ is the relative slip in the hoop direction, θ is the inclined angle of the rib, L is

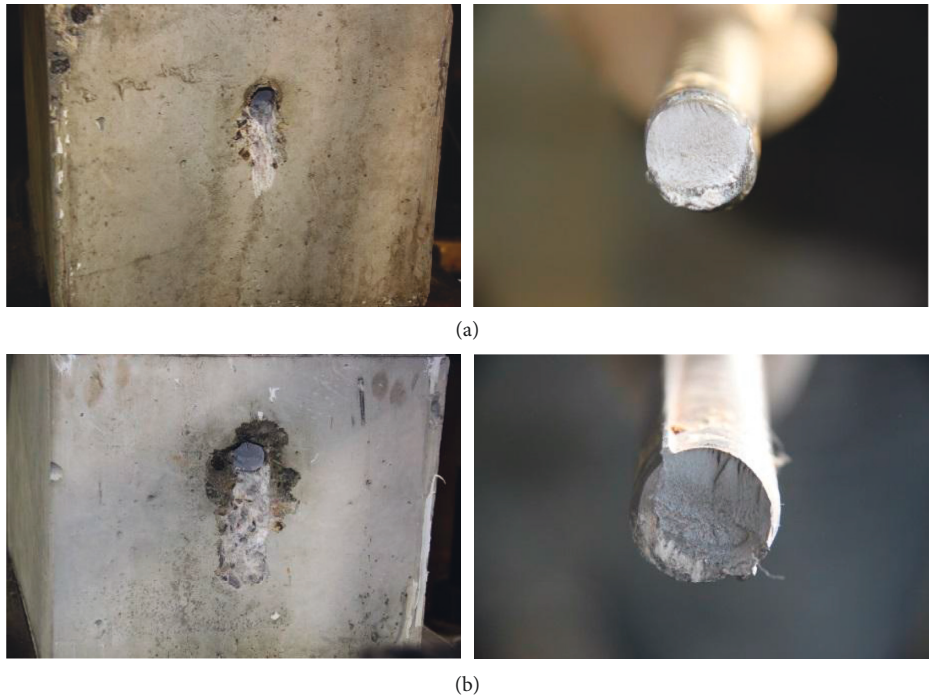

(a)

(b)

Figure 7: Typical failure mode of specimens (a) D20-F and (b) D25-F.

the spacing of the ribs in the axial direction, G_n is the tangential stiffness in the hoop direction, σ_a is the local normal contact stress considering the damage effect, σ_n' is local normal compression stress, and τ_a' is the friction stress along the rib. Details of the model are skipped here, but can be found in the previous work [21].

Experiment results proposed by Maekawa and Qureshi [16] showed that the dowel and pullout behaviors of embedded bar are mutually interactive and interdependent. The pullout behavior is affected by the transverse shear, and the dowel action is in turn affected by the pullout behavior. This mutual dependency is strongly influenced by the local plasticity resulting from the interaction between the interface and the embedded bar. As shown in Figure 10, both micro radial cracks due to axial slip and the localized crushing of the surrounding concrete due to shear displacement can damage the subgrade concrete.

Therefore, in this model, both the local axis strain of rebar and the local compressive strain of concrete are adopted, and the local normal compression stress σ_n' and local normal contact stress σ_a can be expressed as

$$\sigma_n' = \frac{\sigma_n^0}{1 + \varepsilon_s \times 10^{3.5} + \varepsilon_c \times 10^{\lambda_c}},$$
$$\sigma_a = \frac{\sigma_a^0}{1 + \varepsilon_s \times 10^{3.5} + \varepsilon_c \times 10^{\lambda_c}}, \quad (2)$$

where ε_s and ε_c denote the strain of the dowel bar and corresponding concrete, and λ_c is the damage index due to the localized crushing of concrete and is determined as 3.5 according to previous analysis.

Verification of the basic methodology has been conducted by comparing the analysis results with experimental data and previous published models [21]. The distribution characteristics of the curvature and the local axial-bending stress of reinforcing bar are in agreement with previous published results [18, 21].

3.2. Damage Evolution under Fatigue Loads. When the reinforcing bar is subjected to fatigue loads, high-frequency interaction between concrete and steel bar will be caused. The fatigue damage accumulates during the interaction and causes the deterioration of the bond behavior. The process of fatigue damage accumulation actually represents the micro radial cracks and the localized crushing of the surrounding concrete, and it heavily depends on the path of the relative motions between concrete and reinforcing bar. Therefore, a deterioration coefficient χ based on the deformation path could be defined to represent the accumulation of fatigue damage. The effect of fatigue damage on the bond behavior could be considered by reducing the total normal stress σ_n and the bond stress τ_a using the deterioration coefficient χ:

$$\begin{bmatrix} \sigma_{nf} \\ \tau_{af} \end{bmatrix} = \chi \begin{bmatrix} \sigma_n \\ \tau_a \end{bmatrix}, \quad (3)$$

where τ_{af} and σ_{nf} are the bond stress in the axial direction and the total normal stress, considering the fatigue damage, and χ is the damage coefficient which can be computed as

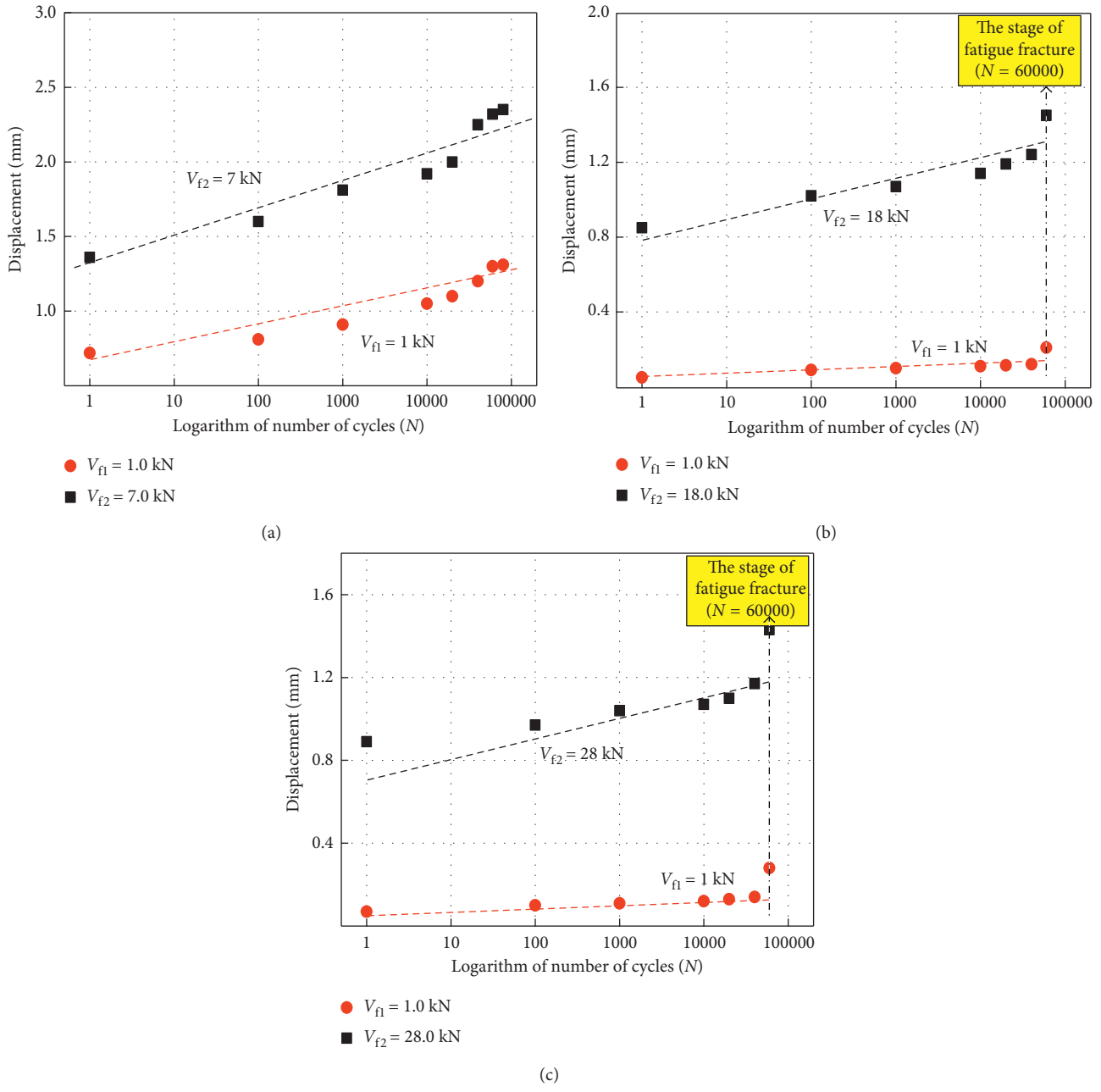

Figure 8: Incremental displacement against the number of fatigue cycles: (a) D12-F; (b) D20-F; (c) D25-F.

$$\chi = \begin{cases} 1 - 0.04 \times \dfrac{1}{10} \log_{10}\left[1 + \sum_j \zeta \left| d\left(\dfrac{\delta_2}{\omega}\right)\right|\right] \geq 0.1, & |\omega| \geq 0.001 \text{ mm} \\ 0, & |\omega| < 0.001 \text{ mm}. \end{cases} \tag{4}$$

In (10), the path of the path of the relative motions between concrete and reinforcing bar is considered by introducing displacement parameters w and δ_2. ζ is the acceleration factor used in numerical integration.

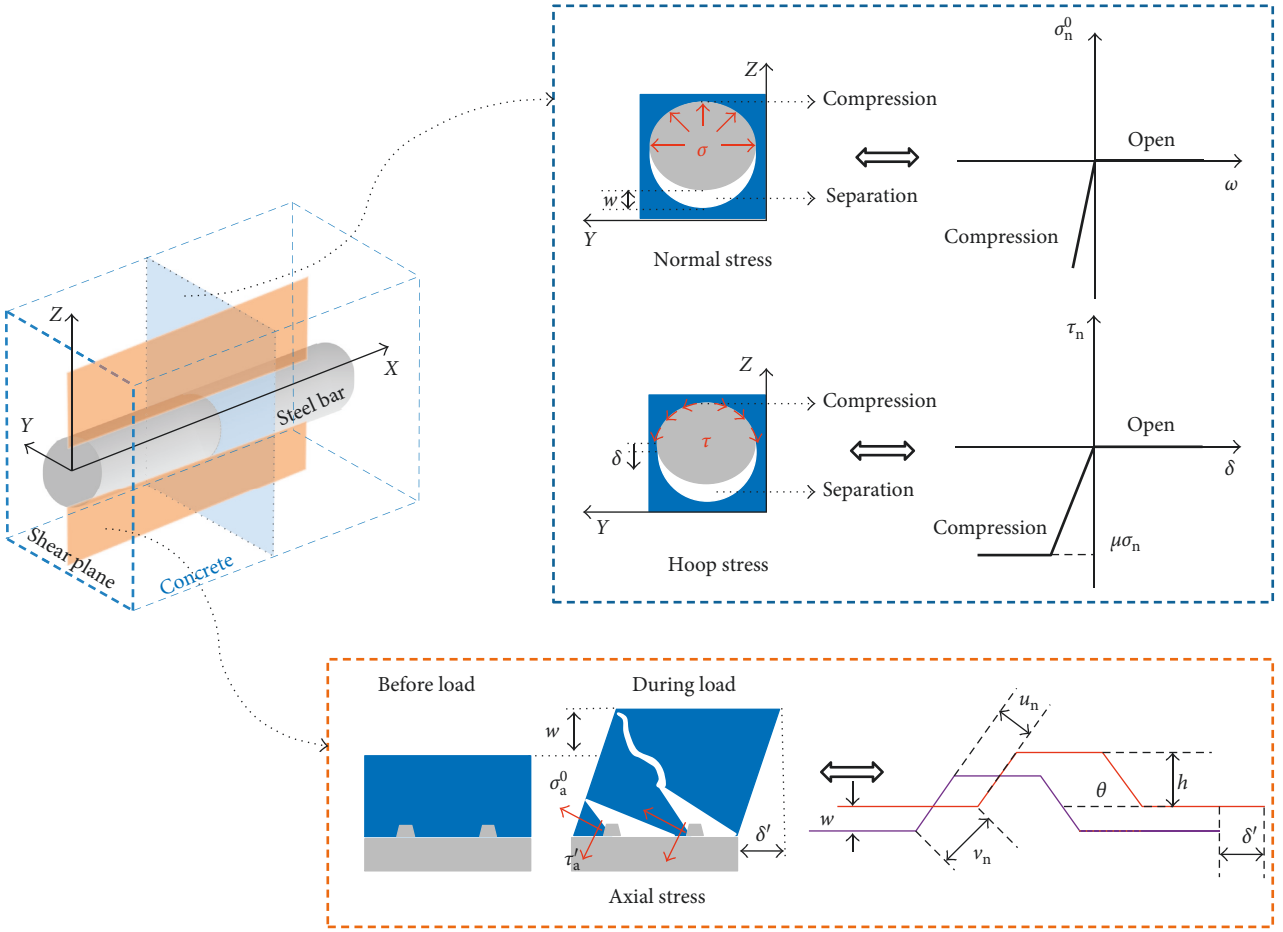

Figure 9: Modelling of the bond in the normal, hoop, and axial direction.

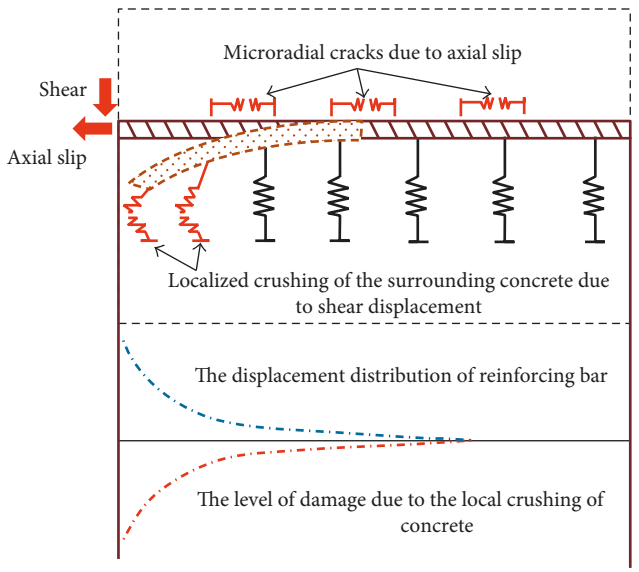

Figure 10: Coupled damage effect of the bong behavior.

The stiffness matrix of the bond model also should be reduced to represent the deterioration effect of the contact stiffness:

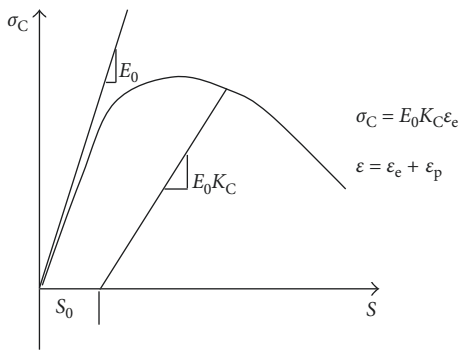

Figure 11: Compression model.

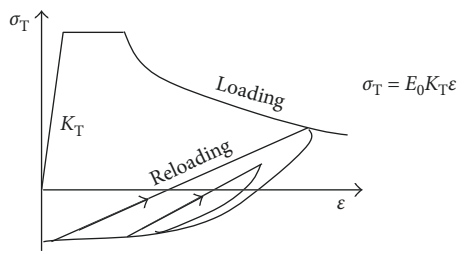

Figure 12: Tension model.

$$K_{\mathrm{f}}^{\mathrm{e}} = \chi K^{\mathrm{e}}, \tag{5}$$

where $K_{\mathrm{f}}^{\mathrm{e}}$ is the stiffness matrix of the bond model, considering the fatigue damage, and $K_{\mathrm{f}}^{\mathrm{e}}$ is the stiffness matrix of the bond model regardless of the fatigue damage.

Altogether, the three-dimensional bond stress field considering the fatigue damage can be computationally summarized as follows:

$$\begin{aligned} \tau_{\mathrm{af}} &= \chi\left[\frac{1}{L}\left(\sigma_L \sin\theta + \tau_L \cos\theta\right)\right], \\ \tau_n &= G_{\mathrm{n}}\delta \le \mu\sigma_{\mathrm{n}}, \\ \sigma_{\mathrm{nf}} &= \chi\left[\frac{1}{L}\left(-\sigma_L \cos\theta + \tau_L \sin\theta + \sigma_{\mathrm{nn}}\right)\right]. \end{aligned} \tag{6}$$

4. Scheme of the Numerical Analysis for Fatigue Load

To simulate the dowel action under combined fatigue shear and pullout tension, the bond model is integrated into the path-dependent integral scheme [22, 25]. In this scheme, fatigue damage of concrete is considered as the time-dependent plasticity and fracturing. The fatigue damage of concrete is formulated in terms of uniaxial compression, tension, and shear, respectively.

As shown in Figure 11, an elastoplastic and fracture model is used to simulate the uniaxial compression behavior of concrete:

$$\begin{aligned} \varepsilon &= \varepsilon_{\mathrm{e}} + \varepsilon_{\mathrm{p}}, \\ \sigma &= E_0 \varepsilon_{\mathrm{e}} K_{\mathrm{c}}, \end{aligned} \tag{7}$$

where ε, ε_{e}, and ε_{p} are the total strain, elastic strain, and plastic strain, respectively; σ is the total stress; E_0 is the initial stiffness; and K_{c} is the fracture parameter which can be computed as

$$\begin{aligned} dK_{\mathrm{c}} &= \left(\frac{\partial K_{\mathrm{c}}}{\partial t}\right)dt + \left(\frac{\partial K_{\mathrm{c}}}{\partial \varepsilon_{\mathrm{e}}}\right)d\varepsilon_{\mathrm{e}}, \\ d\varepsilon_{\mathrm{p}} &= \left(\frac{\partial \varepsilon_{\mathrm{p}}}{\partial t}\right)dt + \left(\frac{\partial \varepsilon_{\mathrm{p}}}{\partial \varepsilon_{\mathrm{e}}}\right)d\varepsilon_{\mathrm{e}}. \end{aligned} \tag{8}$$

Figure 12 shows the tension model of concrete. A simple model is used to represent the tension nonlinearity:

$$\sigma_{\mathrm{T}} = E_0 \varepsilon_{\mathrm{T}} K_{\mathrm{T}}, \tag{9}$$

where σ_{T} is the total tension stress, ε_{T} is the total tension strain, and K_{T} is the tensile fracture parameter that can be defined as

$$dK_{\mathrm{T}} = Hd\varepsilon_{\mathrm{T}} + Fdt + Gd\varepsilon_{\mathrm{T}}, \tag{10}$$

where H is the instantaneous fracture related to tension softening, F is the time-dependent fracture due to creep effect, and G is the fatigue damage.

For the shear fatigue behavior of concrete, a shear transfer model, considering the crack roughness and contact friction, is adopted in this study, as shown in Figure 13. Similar to the deterioration coefficient, a fatigue modification factor is used:

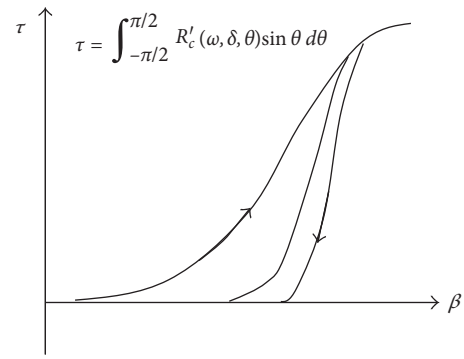

Figure 13: Shear model.

$$\begin{aligned} \tau &= X \cdot \tau_{\mathrm{or}}(\delta_0, \omega_0), \\ X &= 1 - \frac{1}{10}\log_{10}\left(1 + \int \left|d\left(\delta_0/\omega_0\right)\right|\right), \end{aligned} \tag{11}$$

where τ is the transferred shear stress under fatigue loads and δ_0 and ω_0 are the crack and slip, respectively. The fatigue modification X changes with regard to common logarithmic scale.

5. Verification

To verify the proposed bond model, specimens D12-F, D20-F, and D25-F are simulated, and the comparison of the FE analytical results and the experimental data is shown in Figure 14. Both the deterioration of stiffness and the ultimate load due to fatigue damage can be numerically simulated.

In addition, a series of interface-shear experiments are chosen to verify the applicability of the bond model [8]. As shown in Figure 15, 2 specimens with different concrete cover are subjected to cyclic loads. A comparison of the analysis and the experimental results is shown in Figure 16. A good agreement between the analytical and experimental results is confirmed.

6. Conclusions

To predict the force-displacement characteristics (dowel stiffness) and strength of the dowel action under fatigue loads, a series of tests were carried out to determine the mechanism of dowel action fatigue deterioration and the fatigue failure modes. A nonlinear bond model considering the fatigue damage effects was developed. The following conclusions can be drawn from the results:

(1) The accumulated fatigue damage due to the fatigue loads will significantly reduce the ultimate bearing capacity of dowel action. The fatigue deterioration of dowel action should be considered in engineering design to ensure the safety of the structures.

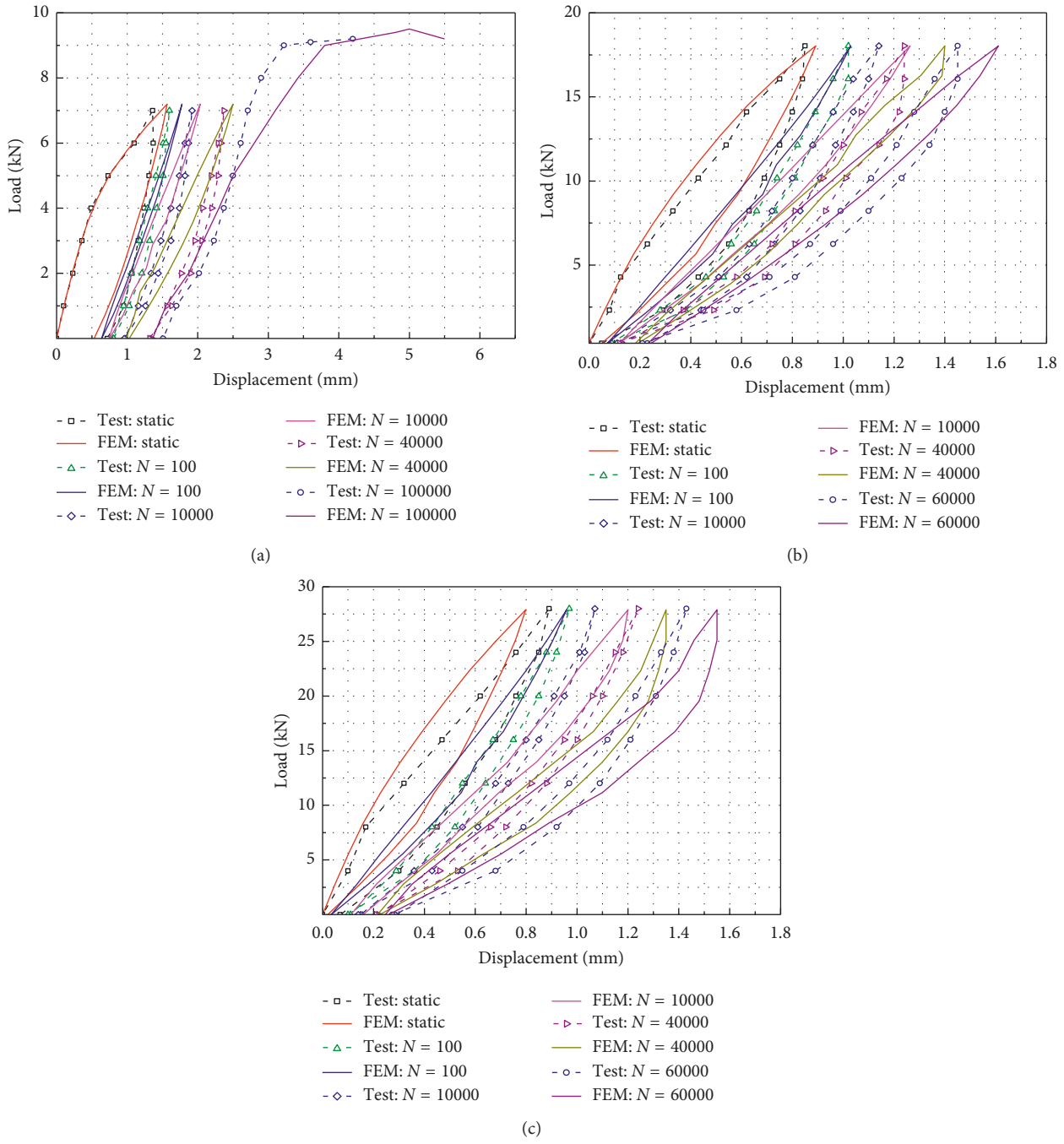

Figure 14: Comparison of FE analysis results and experimental data: (a) D12-F; (b) D20-F; (c) D25-F.

(2) The failure mode of dowel action will transform to fatigue rupture of the dowel bar under serviceability loading state (55% of the static capacity). The fatigue life is determined by the fatigue properties of steel and concrete.

(3) The fatigue damage effect was considered in the model. A deterioration coefficient based on the deformation path is defined to represent the accumulation of fatigue damage.

(4) A systematic experimental verification was performed to demonstrate the versatility of the model, and a reasonable accuracy was found.

Data Availability

The data on figures and tables used to support the findings of this study are included within the article.

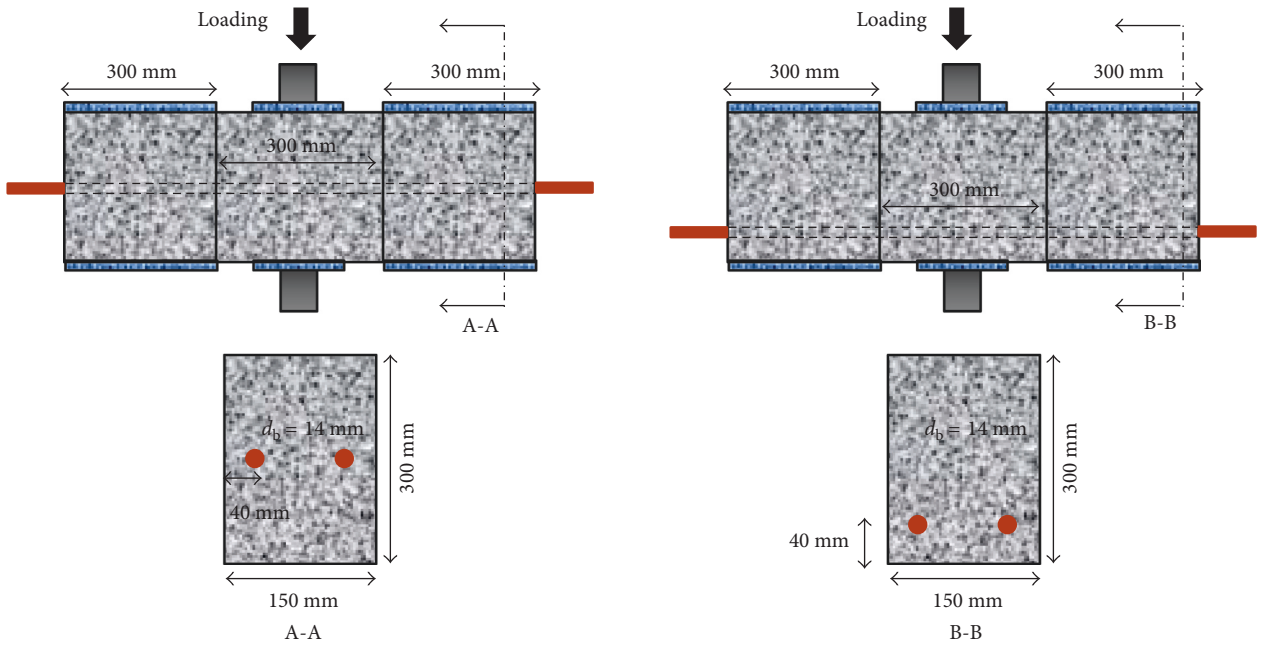

Figure 15: Details of the experiment.

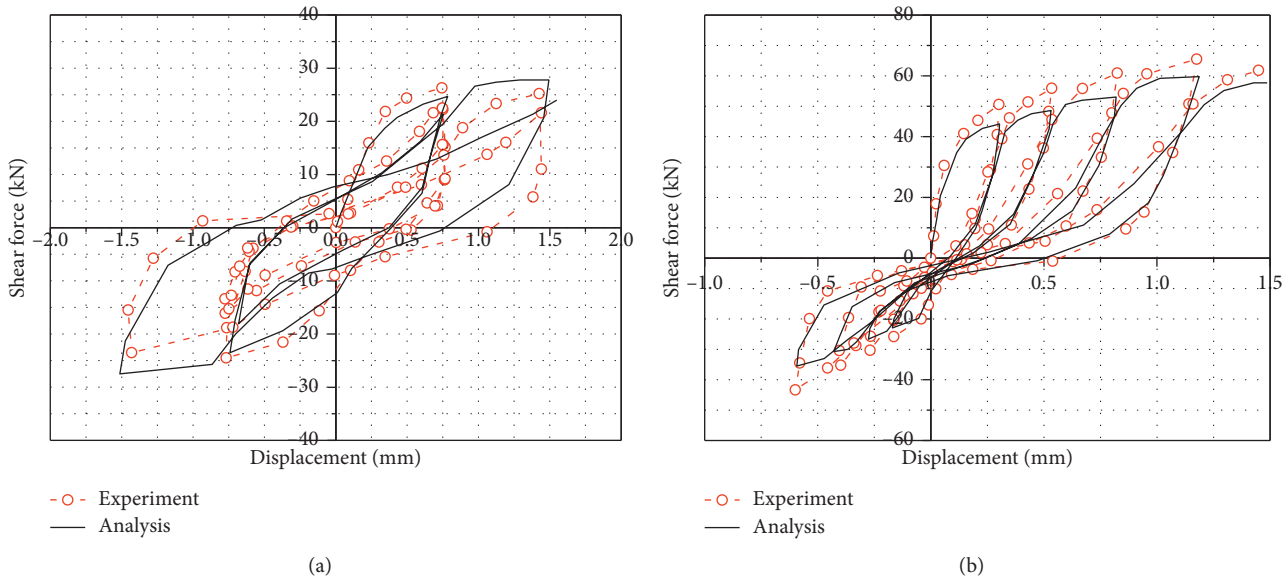

Figure 16: Comparison of FE analysis results and experimental data: (a) specimen A (the concrete cover is 143 mm); (b) specimen B (the concrete cover is 33 mm).

Conflicts of Interest

The authors declare that they have no conflicts of interest.

Acknowledgments

This work was supported by the National Natural Science Foundation of China and the projects of Chongqing Science and Technology Commission (nos. 51709026 and cstc2017jcyjA1662).

References

[1] M. Soltani and K. Maekawa, "Path-dependent mechanical model for deformed reinforcing bars at RC interface under coupled cyclic shear and pullout tension," *Engineering Structures*, vol. 30, no. 4, pp. 1079–1091, 2008.

[2] A. Pavese and D. A. Bournas, "Experimental assessment of the seismic performance of a prefabricated concrete structural wall system," *Engineering Structures*, vol. 33, no. 6, pp. 2049–2062, 2011.

[3] Z. Hu and Z. Guo, "Seismic test and analysis of joints of new precast concrete shear wall structures," *China Civil Engineering Journal*, vol. 45, no. 1, pp. 69–76, 2012.

[4] J. Sun, H. X. Qiu, Y. Yang et al., "Experimental and analytical studies on the deformability of a precast RC shear wall involving bolted connections," *Science China Technological Sciences*, vol. 58, no. 8, pp. 1439–1448, 2015.

[5] P. Soroushian, K. Obaseki, and M. C. Rojas, "Bearing strength and stiffness of concrete under reinforcing bars," *Materials Journal*, vol. 84, no. 3, pp. 179–184, 1987.

[6] P. Soroushian, K. Obaseki, M. C. Rojas et al., "Analysis of dowel bars acting against concrete core," *Journal of the American Concrete Institute*, vol. 83, no. 4, pp. 642–649, 1986.

[7] E. N. Vintzēleou and T. P. Tassios, "Mathematical models for dowel action under monotonic and cyclic conditions," *Magazine of Concrete Research*, vol. 38, no. 134, pp. 13–22, 1986.

[8] E. N. Vintzeleou and T. P. Tassios, "Behavior of dowels under cyclic deformations," *ACI Structural Journal*, vol. 84, no. 1, pp. 18–30, 1987.

[9] A. H. Mattock and N. M. Hawkins, "Shear transfer in reinforced concrete-recent research," *Journal of PCI*, vol. 17, no. 2, pp. 55–75, 1972.

[10] M. Soltani, X. An, and K. Maekawa, "Localized nonlinearity and size-dependent mechanics of in-plane RC element in shear," *Engineering Structures*, vol. 27, no. 6, pp. 891–908, 2005.

[11] L. Xu, T. K. Hai, and L. C. King, "Bond stress-slip prediction under pullout and dowel action in reinforced concrete joints," *ACI Structural Journal*, vol. 111, no. 4, p. 977, 2014.

[12] A. K. H. Kwan, P. L. Ng, and J. Y. K. Lam, "Modelling dowel action of discrete reinforcing bars in cracked," *Energy*, vol. 5, p. 10, 2010.

[13] K. Lundgren, "Bond between ribbed bars and concrete. Part 2: the effect of corrosion," *Magazine of Concrete Research*, vol. 57, no. 7, pp. 383–396, 2005.

[14] K. Lundgren, "Effect of corrosion on the bond between steel and concrete: an overview," *Magazine of Concrete Research*, vol. 59, no. 6, pp. 447–461, 2007.

[15] A. R. Moradi, M. Soltani, and A. A. Tasnimi, "A simplified constitutive model for dowel action across RC cracks," *Journal of Advanced Concrete Technology*, vol. 10, no. 8, pp. 264–277, 2012.

[16] K. Maekawa and J. Qureshi, "Embedded bar behavior in concrete under combined axial pullout and transverse displacement," *Doboku Gakkai Ronbunshu*, vol. 1996, no. 532, pp. 183–195, 1996.

[17] K. Maekawa and J. Qureshi, "Computational model for reinforcing bar embedded in concrete under combined axial pullout and transverse displacement," *Doboku Gakkai Ronbunshu*, vol. 1996, no. 538, pp. 227–239, 1996.

[18] K. Maekawa and J. Qureshi, "Stress transfer across interfaces in reinforced concrete due to aggregate interlock and dowel action," *Doboku Gakkai Ronbunshu*, vol. 1997, no. 557, pp. 159–172, 1997.

[19] F. Shang, X. An, S. Kawai et al., "Open-slip coupled model for simulating three-dimensional bond behavior of reinforcing bars in concrete," *Computers and Concrete*, vol. 7, no. 5, pp. 403–419, 2010.

[20] F. Shang, X. An, T. Mishima et al., "Three-dimensional nonlinear bond model incorporating transverse action in corroded RC members," *Journal of Advanced Concrete Technology*, vol. 9, no. 1, pp. 89–102, 2011.

[21] P. F. Li, X. H. An, S. Q. He et al., "Three-dimensional bond model considering the coupled damage effect for dowel action," *Magazine of Concrete Research*, vol. 69, no. 14, pp. 728–744, 2017.

[22] K. Maekawa, K. Toongoenthong, E. Gebreyouhannes et al., "Direct path-integral scheme for fatigue simulation of reinforced concrete in shear," *Journal of Advanced Concrete Technology*, vol. 4, no. 1, pp. 159–177, 2006.

[23] C. Fujiyama and K. A. Maekawa, "Computational simulation for the damage mechanism of steel-concrete composite slabs under high cycle fatigue loads," *Journal of Advanced Concrete Technology*, vol. 9, no. 2, pp. 193–204, 2011.

[24] C. Fujiyama, X. J. Tang, F. Shang et al., "Residual fatigue life assessment of damaged RC bridge slabs based on site-inspection for cracking: a quantitative discussion," *Advances in Structural Engineering*, vol. 17, no. 4, pp. 481–494, 2014.

[25] K Maekawa and K. F. El-Kashif, "Cyclic cumulative damaging of reinforced concrete in post-peak regions," *Journal of Advanced Concrete Technology*, vol. 2, no. 2, pp. 257–271, 2004.